

EFFICIENT DETERMINATION OF THE NEAR-FIELD IN THE VICINITY OF AN ANTENNA FOR THE ESTIMATION OF ITS SAFETY PERIMETER

J. Laviada, Y. Álvarez-López, and F. Las-Heras

Department of Electrical Engineering
Universidad de Oviedo
Campus Universitario, Gijón, Asturias 33203, Spain

Abstract—The following paper deals with the problem of computing a safety perimeter, i.e., where the electromagnetic field due to a radiating system exceeds a certain electromagnetic value. The flexibility of the source reconstruction method (SRM) is employed to compute the fields almost everywhere around the antenna. Techniques for fast computing of the fields in the spectral and spatial domains exploiting the characteristics of the SRM are considered in order to avoid expensive integrations over the sources surface. Results for a log-periodic antenna and a base station antenna for cellular phone systems are shown, and compared with the usual far-field approximation.

1. INTRODUCTION

After the boom of the cellular phone systems and the consequent installation of base stations, a certain social alarm was created due to the fear of possible human hazards. As a result of this social concern, several studies were carried out in order to evaluate the limits for human exposure. Guidelines were proposed by the ICNIRP [3] establishing the *maximum reference values* in terms of electric field strength, magnetic field strength, and power density for human exposure. These guidelines have been recommended by the European Commission [1] and they have been assumed as officially normative in multiple countries such as Spain [5] and Italy [2]. In the United States, the Federal Communications Commission (FCC) has also provided similar directives for human exposure to electromagnetic fields [4].

For this reason, the volume around an antenna, where the limits are exceeded, has to be delimited to avoid the entry by people. This

Corresponding author: J. Laviada (jlaviada@tsc.uniovi.es).

delimited area, usually approximated by a canonical surface such as a rectangular box or a cylinder, is known as the *safety perimeter*.

The determination of this exclusion volume can be done in an anechoic chamber by measuring the antenna in multiple points determining where the limits are reached. However, this procedure is very time-consuming and it can not be applied if the exclusion volume is larger than the measurement facility.

Several previous works [13, 22, 25] have focused on deriving analytical formulations to estimate the fields in the vicinity of collinear arrays. Although these formulations cover many usual cases of mobile telephony base stations, they are not general and they may not be accurate for many modern antennas.

Another important research line is focused on applying near-field to near-field (NF-NF) transformations to the measured field (e.g., [11, 18, 19]). One of the most important advantages of these methods is that they do not require any assumption regarding the characteristics of the antenna (e.g., assuming a collinear array). Among these techniques, the spherical wave expansion (SWE) is probably the most common because its corresponding measurement range does not introduce truncation errors. This powerful technique is very efficient but it is not able to reconstruct the field inside the minimum sphere enclosing the antenna [15], despite a new formulation combining spherical and plane wave expansion with applications to antenna diagnostics presented in [16, 17]. Another successful attempt to overcome this limitation has been done in [6] for certain class of collinear arrays by exploiting the *a priori* knowledge of the element positions. Therefore, this approach can not be applied in a general case. The rest of the usual NF-NF transformations (e.g., plane to plane techniques) also suffer similar limitations when estimating the field everywhere outside the antenna.

In this paper, we propose a different approach based on the source reconstruction method (SRM) [33] and its three-dimensional application [8], which has been extensively compared with the SWE in [9]. This method calculates a current distribution on an arbitrary domain enclosing the antenna. This current distribution radiates the same field that the antenna outside the reconstruction domain radiates. Although the SRM method involves a computational complexity higher than the NF-NF transformations based on wave mode expansion, the method makes possible to calculate the fields radiated by the antenna not only on the reconstruction surface (e.g., on the radome [30]) but also everywhere outside the reconstruction domain, and it can be applied both to measurements from canonical ranges (such as a plane [26, 34], a cylinder [34] or a sphere [16, 17, 34]) and from arbitrary

acquisition systems. Additionally, several techniques have been recently developed to reduce the computational complexity [10, 28].

A two-dimensional version of the SRM together with a brute-force field computation was employed in [27] to evaluate the exclusion volumes. In this paper, the flexibility of defining an arbitrary 3D reconstruction domain, as well as the shape of the basis functions, will be exploited for the fast computation of the fields radiated in the proximity of the antenna. Since the SRM has been extensively treated in the references [7–9, 27, 29], we will mainly focus on the fast calculation of the near-field once the equivalent currents have been computed. For this purpose, typical approaches are based on adapting acceleration schemes for the method of moments. The most common technique is probably the fast multipole method (FMM) [23] and its multilevel version (MLFMA) [32], whose application to the calculation of the near field has been shown in [20]. However, the technique presented here is adapted from the Conjugated Gradient-Fast Fourier Transform (CG-FFT) [24, 31] instead of FMM due to two main aspects: i) it does not require any special treatment for near interactions; ii) it does not depend on control parameters such as the number of multipoles or integration points. A method also exploiting the invariance of the Green's functions will be presented in the spatial domain. Although the application of these techniques is probably not new for near-field calculation, it has not been previously applied in this context with the SRM to the authors' best knowledge.

Once the field in the vicinity of the antenna has been computed, the determination of the safety perimeter is reduced to finding the isosurface where the limit value is reached. In this paper, we will only consider limits in terms of maximum electric field strength reference values as given in [3]. Nonetheless, we do not foresee any problem in the application to other limits (magnetic field strength or power density).

The paper is arranged as follows. First, the estimation based on the far-field approximation is presented in order to understand its limitations. Next, the determination of the near-field from the equivalent sources is considered. The appropriate setup for the SRM as well as the observation points (in order to take advantage of the Green's function properties) are discussed and the approaches in the spatial and spectral domain are detailed. Next, their computational complexities are numerically estimated and compared with theoretical ones. In order to illustrate and compare the techniques, two examples, one involving a wideband log-periodic antenna and the other a base station antenna using real measured data are given in Section 3. The discussion and conclusions are given in the last section. The paper ends with two

appendices gathering some important numerical aspects regarding the implementation of the spatial and spectral domain approaches.

2. EFFICIENT TECHNIQUES

A first approximation to compute the exclusion volume is to suppose that the field limit falls in the far-field region of the antenna. Thus, the square of the field strength is proportional to the radiation pattern of the antenna:

$$\|\mathbf{E}(R, \theta, \phi)\|^2 = \frac{P_{rad}D(\theta, \phi)}{4\pi R^2} 2\eta, \quad (1)$$

where R is the distance to the antenna, P_{rad} is the power radiated by the antenna, $D(\theta, \phi)$ is the directive gain of the antenna, and, η is the free space impedance.

If we define a limit value for the electric field strength as E_{max} , then the limit of the safety perimeter, for a certain direction, is given by:

$$R(\theta, \phi) = \frac{1}{E_{max}} \sqrt{\frac{P_{rad}D(\theta, \phi) 2\eta}{4\pi}}. \quad (2)$$

Since this formulation is only valid if the antenna distance R is in the far-field region, it is necessary to employ more refined techniques to evaluate the safety perimeters in close proximity of the antenna. However, it is useful to remark that this formulation is accurate for the main lobe of the antenna and high equivalent isotropically radiated power (EIRP) values.

In the remainder of this paper, the safety perimeter will be evaluated numerically from the field calculated on a regular grid. As will be explained later, it is convenient to reconstruct the equivalent sources of the antenna over a rectangular box with the same spacing for their basis functions as for the observation grid (see Fig. 1). It is also important to remark that the maximum spacing for the equivalent sources is $\lambda/2$ [9] and, therefore, the minimum resolution for the field observation grid is also $\lambda/2$.

2.1. Calculation in the Spatial Domain

Free-space Green's functions are invariant with the position of the source, i.e., they only depend on the relative positions of the source and observation points. This enables us to express the field radiated by a certain electric or magnetic current source distribution, $\mathbf{J}(\mathbf{r})$ and $\mathbf{M}(\mathbf{r})$

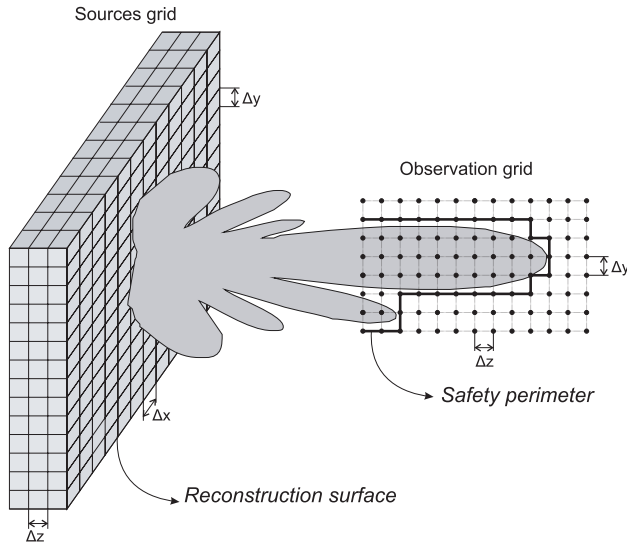


Figure 1. Approximation of the safety perimeter with a regular grid with the same spacing as the source grid. For the sake of clarity, the x -dimension of the observation grid has been omitted.

respectively, in free-space as a convolution of the Green’s functions with the current distribution:

$$\mathbf{E}(\mathbf{r}) = -j\omega\mu\overline{\mathbf{G}}^{(e)}(\mathbf{r}) * \mathbf{J}(\mathbf{r}), \quad (3)$$

$$\mathbf{E}(\mathbf{r}) = \overline{\mathbf{G}}^{(m)}(\mathbf{r}) * \mathbf{M}(\mathbf{r}), \quad (4)$$

where ω is the angular frequency, μ is the free-space magnetic permeability, and $\overline{\mathbf{G}}^{(e)}$ and $\overline{\mathbf{G}}^{(m)}$ are the free-space dyadic Green’s function for electric and magnetic currents [14, 21]:

$$\overline{\mathbf{G}}^{(e)}(\mathbf{r}) = \left(\overline{\mathbf{I}} + \frac{\nabla\nabla}{k_0^2} \right) g(\mathbf{r}), \quad (5)$$

$$\overline{\mathbf{G}}^{(m)}(\mathbf{r}) = -\nabla \times (g(\mathbf{r})\overline{\mathbf{I}}), \quad (6)$$

where k_0 is the wavenumber, $\overline{\mathbf{I}}$ is the unit dyadic, and $g(\mathbf{r})$ is the free-space scalar Green’s function:

$$g(\mathbf{r}) = \frac{1}{4\pi} \frac{e^{-jk_0\|\mathbf{r}\|}}{\|\mathbf{r}\|}. \quad (7)$$

If electric and magnetic currents are considered simultaneously, then the total field is given by the superposition of the fields from (3) and (4).

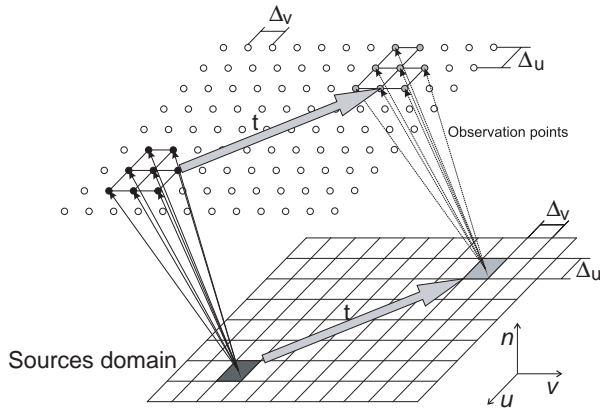


Figure 2. Translation invariance for a current distribution on a plane.

This property means that if a set of sources is moved a direction \mathbf{t} , then the field radiated is also moved in the same direction. Thus, if the same spacing is used for the sources and observation grids, it is possible to evaluate the field due to a certain basis function by just translating the field (previously calculated) due to another basis function (see Fig. 2). In other words, it is possible to compute the field in the entire observation grid by just calculating the field due to one basis function and appropriately translating (and weighting) this field. This fact, together with the flexibility of choice for the basis functions in the SRM, will be exploited to quickly compute the field in the vicinity of the antenna.

The first step in this strategy is to employ a reconstruction domain equal to a *rectangular box* enclosing the radiating system. The surface of this box is discretized into equal-sized rectangles where pulse basis functions are employed to expand both magnetic and electric currents. In order to model the entire tangential current, two orthogonal basis functions for each kind of current are placed on each rectangle. The rectangles are chosen to have the same length in a given direction. This way, the problem is reduced to computing the field radiated for each face of the rectangular box.

In order to take advantage of this invariance property, the field will be evaluated in a three-dimensional grid with the same spacing as the source grid. Let us assume that the currents on a face belonging to the plane described by two orthogonal vectors \hat{u} and \hat{v} are expanded using N_u basis functions in the u -direction and N_v basis functions in the v -direction. It will be also assumed that N_u and N_v are odd and that the center of the face is placed at the origin of the coordinates

system. Hence, currents are expressed as:

$$\begin{aligned} \mathbf{J}(\mathbf{r}) &= \sum_n \sum_m \alpha_{nm}^{(u,e)} \mathbf{f}^{(u)}(\mathbf{r} - n\Delta_u \hat{u} - m\Delta_v \hat{v}) \\ &\quad + \sum_n \sum_m \alpha_{nm}^{(v,e)} \mathbf{f}^{(v)}(\mathbf{r} - n\Delta_u \hat{u} - m\Delta_v \hat{v}), \end{aligned} \quad (8)$$

$$\begin{aligned} \mathbf{M}(\mathbf{r}) &= \sum_n \sum_m \alpha_{nm}^{(u,m)} \mathbf{f}^{(u)}(\mathbf{r} - n\Delta_u \hat{u} - m\Delta_v \hat{v}) \\ &\quad + \sum_n \sum_m \alpha_{nm}^{(v,m)} \mathbf{f}^{(v)}(\mathbf{r} - n\Delta_u \hat{u} - m\Delta_v \hat{v}), \end{aligned} \quad (9)$$

where Δ_u and Δ_v are the spacings in the u and v -direction, respectively, $\alpha_{nm}^{(\alpha,\beta)}$ are the weights (calculated with the SRM) for the basis function in the n - m position, in the u - and v -direction, respectively, $\mathbf{J}(\mathbf{r})$ and $\mathbf{M}(\mathbf{r})$ are the electric and magnetic currents, respectively, and $\mathbf{f}^{(u)}$ and $\mathbf{f}^{(v)}$ are pulses with u - and v -components, respectively. The index n ranges from $-(N_u - 1)/2$ to $(N_u - 1)/2$ and the index m ranges from $-(N_v - 1)/2$ to $(N_v - 1)/2$.

Let us first consider only the field radiated by the electric currents with u -component. Then, the electric field radiated by $\mathbf{J}(\mathbf{r})$ can be calculated by inserting (8) in (3):

$$\mathbf{E}(\mathbf{r}) = \sum_n \sum_m \alpha_{nm}^{(u,e)} \mathbf{E}_0^{(u,e)}(\mathbf{r} - n\Delta_u \hat{u} - m\Delta_v \hat{v}), \quad (10)$$

where \mathbf{E}_0 is the field radiated by the basis function in the center of the face ($n = 0$ and $m = 0$),

$$\mathbf{E}_0^{(u,e)}(\mathbf{r}) = -j\omega\mu\bar{\mathbf{G}}^{(e)}(\mathbf{r}) * \mathbf{f}^{(u)}(\mathbf{r}). \quad (11)$$

Finally, the field on a grid contained in a plane described by the vectors \hat{u} and \hat{v} and the point \mathbf{r}_0 can be computed as:

$$\begin{aligned} &\mathbf{E}(\mathbf{r}_0 + n'\Delta_u \hat{u} + m'\Delta_v \hat{v}) \\ &= \sum_n \sum_m \alpha_{nm}^{(u,e)} \mathbf{E}_0^{(u,e)}(\mathbf{r}_0 - (n - n')\Delta_u \hat{u} - (m - m')\Delta_v \hat{v}) \\ &= \sum_n \sum_m \alpha_{nm}^{(u,e)} \mathbf{E}_{d0}^{(u,e)}[n - n'] [m - m'], \end{aligned} \quad (12)$$

where $\mathbf{E}_{d0}^{(u,e)}[n][m]$ is the sample of the field radiated by $\mathbf{f}^{(u)}(\mathbf{r})$ at the observation point $\mathbf{r} = \mathbf{r}_0 - n\Delta_u \hat{u} - m\Delta_v \hat{v}$,

$$\mathbf{E}_{d0}^{(u,e)}[n][m] = \mathbf{E}_0^{(u,e)}(\mathbf{r}_0 - n\Delta_u \hat{u} - m\Delta_v \hat{v}). \quad (13)$$

Thus, it is only necessary to evaluate the field due to the basis function at the center of the face and, after that, the computation can be

performed without further integrations in the sources domain. A similar formulation can be followed for the other component of the electric current and for both components of the magnetic currents. Thus, the total field is:

$$\begin{aligned} \mathbf{E}(\mathbf{r}_0 + n' \Delta_u \hat{u} + m' \Delta_v \hat{v}) = & \sum_n \sum_m \alpha_{nm}^{(u,e)} \mathbf{E}_{d0}^{(u,e)} [n - n'] [m - m'] \\ & + \sum_n \sum_m \alpha_{nm}^{(v,e)} \mathbf{E}_{d0}^{(v,e)} [n - n'] [m - m'] \\ & + \sum_n \sum_m \alpha_{nm}^{(u,m)} \mathbf{E}_{d0}^{(u,m)} [n - n'] [m - m'] \\ & + \sum_n \sum_m \alpha_{nm}^{(v,m)} \mathbf{E}_{d0}^{(v,m)} [n - n'] [m - m'], \end{aligned} \quad (14)$$

where:

$$\mathbf{E}_{d0}^{(v,e)} [n] [m] = -j\omega\mu \overline{\mathbf{G}}^{(e)}(\mathbf{r}) * \mathbf{f}^{(v)}(\mathbf{r}) \Big|_{\mathbf{r}=\mathbf{r}_0 - n\Delta_u \hat{u} - m\Delta_v \hat{v}}, \quad (15)$$

$$\mathbf{E}_{d0}^{(u,m)} [n] [m] = \overline{\mathbf{G}}^{(m)}(\mathbf{r}) * \mathbf{f}^{(u)}(\mathbf{r}) \Big|_{\mathbf{r}=\mathbf{r}_0 - n\Delta_u \hat{u} - m\Delta_v \hat{v}}, \quad (16)$$

$$\mathbf{E}_{d0}^{(v,m)} [n] [m] = \overline{\mathbf{G}}^{(m)}(\mathbf{r}) * \mathbf{f}^{(v)}(\mathbf{r}) \Big|_{\mathbf{r}=\mathbf{r}_0 - n\Delta_u \hat{u} - m\Delta_v \hat{v}}. \quad (17)$$

It is important to remark that in order to evaluate all the terms in the sums of (14), it is necessary calculate the fields radiated by the centered basis functions not only in the original observation grid but also on an extension with N_u and N_v points for the u - and v -directions, respectively. The computation of these variables can be accelerated using the symmetry properties described in Appendix A.

Although this approach avoids evaluating the integration in the entire reconstruction surface thus saving time, its complexity is the same as in the case of direct integration, i.e., $\mathcal{O}(N_{obs} N_{sou})$, where N_{obs} is the number of observation points and N_{sou} is the number of source points.

2.2. Calculation in the Spectral Domain

As has been shown previously, it is possible to take advantage of the invariance property of the Green's functions in free-space to speed up the computation of the field on a grid. If the same spacing for sources and observation grid is employed, it is also possible to perform this calculation on the spectral domain by exploiting the advantages of the fast Fourier transform (FFT).

If we consider the Fourier transform of the electric field given by (3) at the spectral point $\mathbf{k} = k_x\hat{x} + k_y\hat{y} + k_z\hat{z}$, it yields:

$$\tilde{\mathbf{E}}(\mathbf{k}) = \int_V \mathbf{E}(\mathbf{r}) e^{-j\mathbf{k}\cdot\mathbf{r}} dV = -j\omega\mu \tilde{\mathbf{G}}^{(e)}(\mathbf{k}) \cdot \tilde{\mathbf{J}}(\mathbf{k}), \quad (18)$$

where $\tilde{\mathbf{G}}^{(e)}$ is the Fourier transform of $\overline{\mathbf{G}}^{(e)}$ [21],

$$\tilde{\mathbf{G}}^{(e)} = \left(\overline{\mathbf{I}} - \frac{1}{k_0^2} \mathbf{k}\mathbf{k} \right) \tilde{g}(\mathbf{k}), \quad (19)$$

and $\tilde{g}(\mathbf{k})$ is the Fourier transform of the free-space scalar Green's function,

$$\tilde{g}(\mathbf{k}) = \frac{1}{k_x^2 + k_y^2 + k_z^2 - k_0^2}. \quad (20)$$

$\tilde{\mathbf{J}}(\mathbf{k})$ is the Fourier Transform on the electric currents in (8). In a similar fashion, the Fourier transform of (4) yields:

$$\tilde{\mathbf{E}}(\mathbf{k}) = -j\tilde{g}(\mathbf{k}) \mathbf{k} \times \tilde{\mathbf{M}}(\mathbf{k}) = \tilde{\mathbf{G}}^{(m)} \cdot \tilde{\mathbf{M}}(\mathbf{k}), \quad (21)$$

where $\tilde{\mathbf{G}}^{(m)}$ is the Fourier transform of $\overline{\mathbf{G}}^{(m)}$, which can be expressed as

$$\tilde{\mathbf{G}}^{(m)} = -j\tilde{g}(\mathbf{k}) \begin{pmatrix} 0 & -k_z & k_y \\ k_z & 0 & -k_x \\ -k_y & k_x & 0 \end{pmatrix} \quad (22)$$

and $\tilde{\mathbf{M}}(\mathbf{k})$ is the Fourier Transform of the magnetic currents.

Equations (18) and (21) enable us to calculate the spectrum of the electric field for any spectral point \mathbf{k} . Hence, it is possible to recover the electric field at any point by performing an inverse Fourier transform:

$$\mathbf{E}(\mathbf{r}) = \left(\frac{1}{2\pi} \right)^3 \int_{k_x} \int_{k_y} \int_{k_z} \tilde{\mathbf{E}}(\mathbf{k}) e^{j\mathbf{k}\cdot\mathbf{r}} dk_x dk_y dk_z. \quad (23)$$

This expression can be evaluated on a regular grid in order to recover the field on a spatial grid via FFT. However, it is convenient to consider some numerical aspects to avoid aliasing problems. These considerations are detailed in Appendix B.

The complexity of this spectral domain approach for an observation grid with N_{obs} points and N_{sou} sources is $\mathcal{O}((N_{sou} + N_{obs}) \log(N_{sou} + N_{obs}))$ (see Appendix B). Thus, the spectral domain approach has greater computational complexity than the spatial domain approach regarding the number of observation points. Nevertheless, if the number of sources and the number of observation

points are similar $N_{obs} \approx N_{sou}$, then the complexity is reduced from $\mathcal{O}(N_{obs}^2)$ to $\mathcal{O}(N_{obs} \log N_{obs})$. This fact was already observed when the MLFMA was employed for fast field computation [20]. In the results section, it is shown how similar N_{obs} and N_{sou} values should be used to take advantage of this approach.

It is important to remark that this method is based on performing the numerical convolution related to (3) and (4) via an FFT (see Appendix B for further details) and, therefore, it will yield the same results as we would obtain in the case of using the direct method or the method in the spatial domain.

2.3. Computational Complexities

In order to empirically check the computational complexity of the previous approaches, we will perform two kinds of analyses varying the number of observation points and the number of sources. All the times shown in this paper are measured on a workstation equipped with an AMD Opteron 880 at 2.4 GHz and 64 GB of RAM memory.

For the first case, we consider a 31×31 grid that supports 1922 basis functions for electric currents and the same number for magnetic currents. The observation grid is composed of $11 \times 11 \times N_z$ points, where N_z is the number of points along the z -direction that are going to be progressively increased through the analysis.

The results for both methods are compiled in Fig. 3 with good agreement with the theoretical complexities. Thus, the spectral domain has a higher computational complexity in the asymptotic limit.

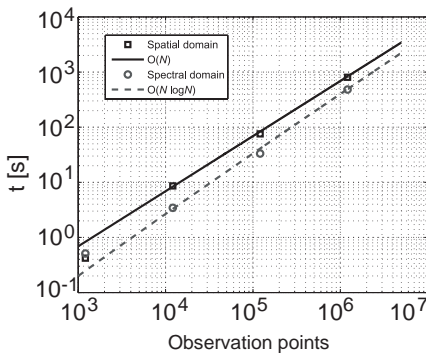


Figure 3. Time complexity versus the number of observation points.

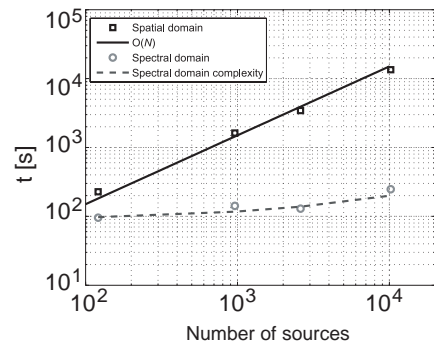


Figure 4. Time complexity versus the number of sources.

Despite this, the spectral domain is slightly faster for the sizes of the problems under consideration here.

Figure 4 shows the results of the complexity when the number of sources is increased and the number of observation points remains fixed. In this case, we consider an observation grid with $211 \times 211 \times 211$ points, while the sources are placed on a square grid with variable size in the XY plane. In the case of the spatial domain approach, the computational time has a linear dependence on the number of sources as predicted by the theory. On the other hand, the time complexity of the spectral domain approach does not suffer a significant change with the number of sources for the range under consideration. The increase in computational time is due to the increase in the observation points to avoid aliasing problems (see Appendix B). This change in computational time is in good agreement with the theoretical complexity given by $\mathcal{O}((N_{sou} + N_{obs}) \log(N_{sou} + N_{obs}))$ and labelled as ‘‘Spectral domain complexity’’ in Fig. 4.

3. NUMERICAL RESULTS

3.1. Log-periodic Antenna

In our first example, we consider the analysis of a wideband antenna to observe the differences of the safety perimeters at different frequencies. For this purpose, we consider the logperiodic antenna analyzed in [29] at 1030 MHz, 1800 MHz and 2500 MHz. Maximum root mean square (RMS) electric field strengths according to [3] as well as the directivity of the antenna are compiled in Table 1.

The antenna is surrounded by a 30 cm \times 2 cm \times 60 cm rectangular box that is discretized employing a 11, 1 and 21 pulses for the x , y , and z , directions, respectively. Thus, the size of the pulses ranges from 0.07λ to 0.23λ . The iterative algorithm employed in the SRM [8] is stopped when the root mean square error between the measured field and the field radiated by the sources is less than 0.1% for two consecutive iterations. Table 2 contains the employed observation

Table 1. Directivity for the logperiodic antenna and maximum electric fields values according to [3].

f (MHz)	D (dBi)	Max E_{rms} (V/m)
1030	8.6	44.1
1800	9.0	58.3
2500	9.4	61

Table 2. Setup of the SRM to compute the currents of the logperiodic antenna.

f (MHz)	Obs. points	iter.	t (s)
1030	21,960	16	528
1800	32,760	17	1037
2500	8,280	20	220

points, the required number of iterations, and the total time employed by the SRM. In order to perform the analysis, the equivalent currents amplitude has been scaled to radiate with an EIRP equals to 100 W.

It is important to remark that the EIRP is a far-field measure and, therefore, it is not significant close to the antenna. However, this parameter is widespread to specify the power radiated by an antenna. For that reason, we have chosen to specify the power radiated by the antennas described in this paper in terms of the EIRP.

The observation grid is chosen to include the reconstruction surface and the safety perimeter calculated using the far-field approximation. Although we estimate these observation grids only for the worst case that corresponds to 1030 MHz, it is also possible to make finer adjustments by changing the grid size with the frequency. Values were rounded to the next 0.5 m multiple in order to have a safety margin. Thus, the values for the x , y and z axis ranges from -1 m, to 1 m, -0.5 m to -0.5 m, and -0.5 m to 1.5 m, respectively.

Safety perimeters are calculated using both spatial and spectral domains without visible discrepancies. For the sake of clarity, only the results from the spectral domains will be shown. These approaches consume 66 s in the spatial domain and 19 s in the spectral domain versus the 344 s for the direct calculation.

The safety perimeters are shown in Fig. 5. Although the far-field approximation provides more conservative safety perimeters in the main lobe at 1030 MHz and 1800 MHz, i.e., the real safety perimeter is closer to the antenna than the provided by the far-field approximation, this is not the case at 2500 MHz where the approximation yields a smaller exclusion volume than the exact near field calculated with the SRM. One of the reasons for this behaviour is that the safety perimeter calculated with (2) tends to become smaller if the maximum electric field strength is increased, as happens for the considered cases. Thus, the far-field approximation becomes inaccurate and the offset from the origin of the antenna also plays a key role. Although the difference is only 4 cm in the maximum radiation direction, it is important to check the far-field approximation in those close cases.

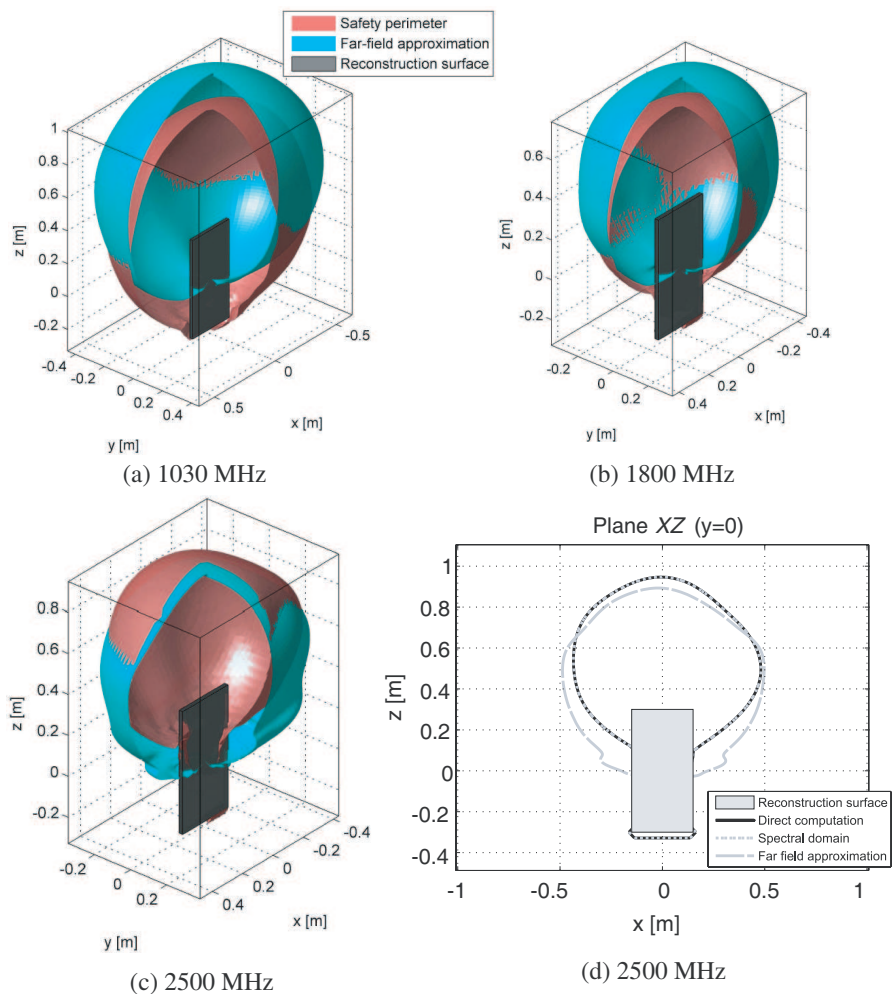


Figure 5. Safety perimeters for the logperiodic antenna at several frequencies. The first quadrant is omitted for proper visualization. The safety perimeter contour in the plane $y = 0$ is also shown for the sake of clarity.

For the rest of directions out of the main lobe, far-field approximation still provides good estimations of the maximum safe distances except for the back radiation ($\theta > \pi/2$) where the radiation close to the antenna is not correctly modeled by the far-field approximation. It is especially visible at 1030 MHz where the safety perimeter is larger for this direction.

3.2. Base Station Antenna

The next example is a base transceiver station (BTS) antenna working at 1800 MHz (DCS band). The gain of this antenna is 12 dB and the size of the radome is $0.2\text{ m} \times 1.6\text{ m} \times 0.1\text{ m}$. Equivalent sources are reconstructed over a surface fitting the radome and using a grid size with 3, 21 and 3 pulses for the x , y and z directions, respectively

In order to reconstruct the currents, the radiation pattern of the antenna was measured using 21,960 acquisition points in a spherical range at 5 m. The same stop condition as before is used and convergence is reached after 11 iterations. The total time to reconstruct the sources is 176 s.

The safety perimeters are computed for several EIRP values and are compiled in Table 3. The observation grid is again chosen to include the reconstruction surface and the safety perimeter calculated from the far-field approximation. The dimensions of this box are also rounded to the next 0.5 m multiple. The range of values for the observation grid as well as the resulting number of observation points for each direction are also shown in Table 3.

Table 4 contains the computational time results for the aforementioned EIRP values. In this case, the time for the spatial and spectral domain techniques are very close enabling the calculation for more than 400,000 observation points in less than 40 s.

Safety perimeters for EIRP equal to 800 W and 3200 W are shown in Fig. 6 for the limit RMS value $E_{rms} = 58.3\text{ V/m}$ following the [3] guidelines. Graphical inspection reveals that the far-field

Table 3. Grid sizes for the BTS working at different EIRPs.

EIRP (Watts)	x (m)	y (m)	z (m)	$N_x \times N_y \times N_z$
800	$[-1.5, 1.5]$	$[-1.0, 3.0]$	$[-1.0, 1.0]$	$47 \times 121 \times 27$
1600	$[-2.0, 2.0]$	$[-1.0, 4.0]$	$[-1.0, 1.0]$	$61 \times 151 \times 27$
3200	$[-2.5, 2.5]$	$[-1.0, 6.0]$	$[-1.0, 1.0]$	$77 \times 211 \times 27$

Table 4. Time values for the Table 2.

EIRP (Watts)	Direct	Spatial domain	Spectral domain
800	101 s	15 s	14 s
1600	163 s	21 s	21 s
3200	287 s	34 s	38 s

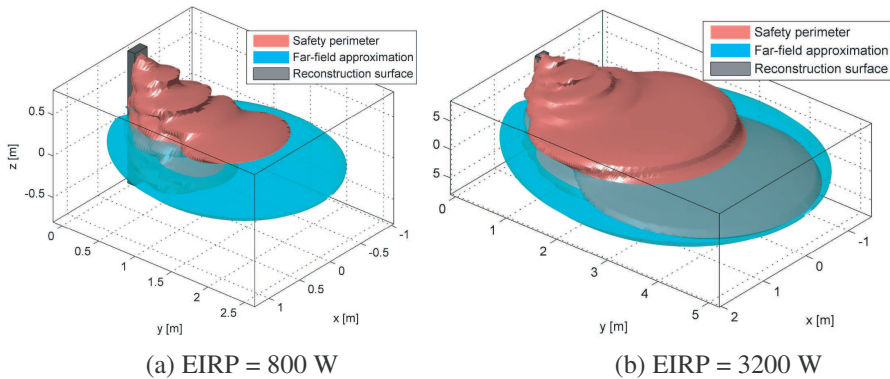


Figure 6. Safety perimeters for the BTS antenna for two different EIRPs.

approximation could be used for large EIRP values where the safety perimeter is closer to the beginning of the far-field area. If the EIRP values are low and, therefore the safety perimeter is closer to the antenna, radiation is not so directive. Thus, the far-field approximation is more conservative for the main lobe but not for the rest of the directions.

4. CONCLUSION

A safety perimeter can be efficiently evaluated with an appropriate setup of the source reconstruction method. From those sources, electromagnetic fields can be quickly computed on an observation grid where the safety perimeter is to be calculated. This calculation has been done by exploiting the invariance property of the Green's function in the spatial and spectral domains. For the spatial domain approach, computational times has a linear dependence on the number of observation points. Thus, it is attractive for problems where many observation points are involved. On the other hand, the spectral domain takes advantage of efficient FFT implementations and it has been demonstrated to be faster or very competitive for the range of problems considered here. The validity of the results from the far-field approximation depends on the desired degree of accuracy.

ACKNOWLEDGMENT

This work has been supported by Ministerio de Ciencia e Innovación of Spain/FEDER under projects TEC2008-01638/TEC (INVENTA)

and CONSOLIDER-INGENIO CSD2008-00068 (TERASENSE); by Unión Europea-Fondo Europeo de Desarrollo Regional under project EQP06-015; by Gobierno del Principado de Asturias-Plan de Ciencia y Tecnología (PCTI)/FEDER-FSE under grants BP06-101/BP06-155 and by Cátedra Telefónica- Universidad de Oviedo.

APPENDIX A. NUMERICAL CONSIDERATIONS FOR THE SPATIAL DOMAIN

Computation of the values in (13)–(17) correspond to the field radiated by a basis function at the origin and evaluated in the position $\mathbf{r} = \mathbf{r}_0 - n\Delta_u\hat{u} - m\Delta_v\hat{v}$ can be accelerated employing some symmetry properties for the u - and v -components of the field. These properties are compiled in the following equations:

$$\hat{u} \cdot \mathbf{E}_{d0}^{(u,e)}[-n][m] = \hat{u} \cdot \mathbf{E}_{d0}^{(u,e)}[n][m], \quad (\text{A1})$$

$$\hat{v} \cdot \mathbf{E}_{d0}^{(u,e)}[n][-m] = -\hat{v} \cdot \mathbf{E}_{d0}^{(u,e)}[n][m], \quad (\text{A2})$$

$$\hat{u} \cdot \mathbf{E}_{d0}^{(v,e)}[-n][m] = -\hat{u} \cdot \mathbf{E}_{d0}^{(v,e)}[n][m], \quad (\text{A3})$$

$$\hat{v} \cdot \mathbf{E}_{d0}^{(v,e)}[n][-m] = \hat{v} \cdot \mathbf{E}_{d0}^{(v,e)}[n][m], \quad (\text{A4})$$

$$\hat{u} \cdot \mathbf{E}_{d0}^{(u,m)}[-n][m] = -\hat{u} \cdot \mathbf{E}_{d0}^{(u,m)}[n][m], \quad (\text{A5})$$

$$\hat{v} \cdot \mathbf{E}_{d0}^{(u,m)}[n][-m] = \hat{v} \cdot \mathbf{E}_{d0}^{(u,m)}[n][m], \quad (\text{A6})$$

$$\hat{u} \cdot \mathbf{E}_{d0}^{(v,m)}[-n][m] = \hat{u} \cdot \mathbf{E}_{d0}^{(v,m)}[n][m], \quad (\text{A7})$$

$$\hat{v} \cdot \mathbf{E}_{d0}^{(v,m)}[n][-m] = -\hat{v} \cdot \mathbf{E}_{d0}^{(v,m)}[n][m]. \quad (\text{A8})$$

Therefore, it is only necessary to compute the E_{d0} values for $n \geq 0$ and $m \geq 0$ reducing by approximately four times the time employed by this stage.

APPENDIX B. NUMERICAL CONSIDERATIONS FOR THE SPECTRAL DOMAIN

If the field spectrum $\tilde{\mathbf{E}}(\mathbf{k})$ is sampled in order to employ the FFT to recover the field in the spatial domain, the results will suffer aliasing problems. This can be avoided by applying a window in the spatial domain to the Green's functions [24]. However, the evaluation of the windowed version of the Green's Functions in the spectral domain involves a convolution between the analytical expressions (19) and (22), and the Fourier transform of the window. Since this operation can be very time-consuming, we overcome this drawback by sampling the windowed Green's function at the points where the field is to be

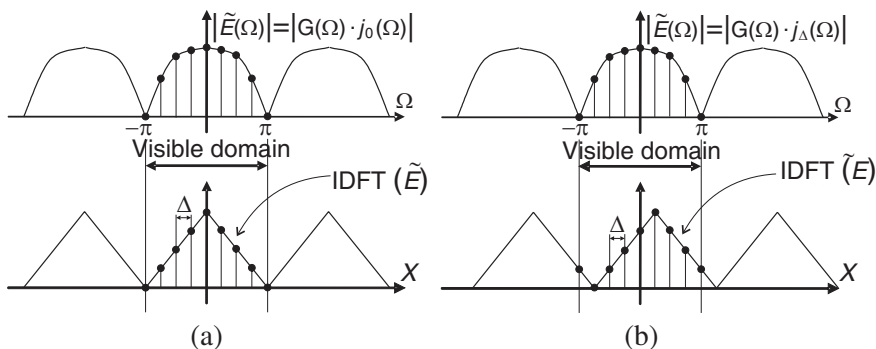


Figure B1. Spatial aliasing.

calculated and the FFT is applied to these samples. In other words, we compute numerically the Fourier transform of the windowed Green’s function.

A similar procedure is carried out to compute the Fourier transform of the currents. However, if pulses are used as basis functions, then this Fourier transform can still be calculated analytically.

Once the samples of the Fourier transforms of the Green’s functions and the currents have been calculated, then the samples of the electric field can be computed by the product of both. It is important to remark that if a basis function is moved one unit in the grid, then the recovered field is also moved in the same direction with a cyclic periodicity in the observation grid. This has been illustrated in Fig. B1 for the one-dimensional case where DFT and IDFT stands for Discrete Time Fourier Transform and Inverse Discrete Time Fourier Transform, respectively. Therefore, if a $N_u \times N_v$ grid is considered, then the observation grid must be extended N_u and N_v cells in the u - and v -directions in order to avoid this spatial aliasing. These extended points will be discarded once the field has been recovered. Hence, the computational complexity and required computing time for this approach are proportional to $\mathcal{O}((N_{sou} + N_{obs}) \log(N_{sou} + N_{obs}))$.

Finally, we would like to remark that in order to numerically evaluate (5) and (6), it is convenient to use more suitable expressions

such as the following ones:

$$\overline{\mathbf{G}}^{(e)}(\mathbf{r}) = \frac{1}{k_0^2} \left(\overline{\mathbf{I}} G_1(r) + \frac{1}{r^2} G_2(r) \mathbf{r} \mathbf{r} \right) e^{-jk_0 r}, \quad (\text{B1})$$

$$\overline{\mathbf{G}}^{(m)}(\mathbf{r}) = G_3(r) \begin{pmatrix} 0 & -z & y \\ z & 0 & -x \\ -y & x & 0 \end{pmatrix} \frac{1}{r} e^{-jk_0 r}, \quad (\text{B2})$$

where $r = \|\mathbf{r}\|$ and G_1 , G_2 and G_3 [12] are given by:

$$G_1(r) = \frac{-1 - jk_0 r + k_0^2 r^2}{4\pi r^3}, \quad (\text{B3})$$

$$G_2(r) = \frac{3 + 3jk_0 r - k_0^2 r^2}{4\pi r^3}, \quad (\text{B4})$$

$$G_3(r) = \frac{-1 - jk_0 r}{4\pi r^2}. \quad (\text{B5})$$

REFERENCES

1. Council recommendation of 12 July 1999 on the limitation of exposure of the general public to electromagnetic fields (0 Hz to 300 GHz), *Official J. European Community L1999*, 59, 1999.
2. Decree 10 september 1998, No. 381. regolamento recante norme per la determinazione dei tetti di radiofrequenza compatibili con la salute umana. *Gazzetta Ufficiale della Repubblica Italiana*, Vol. 257, 9–14, November 1998.
3. ICNIRP guidelines for limiting time-varying electric, magnetic and electromagnetic fields (up to 300 GHz), *Health Phys.*, Vol. 74, No. 4, 494–522, April 1998.
4. *Local Government Official's Guide to Transmitting Antenna RF Emission Safety: Rules, Procedures, and Practical Guidance.*, Federal Communication Commission/Local and State Government Advisory Committee, 2000.
5. Real decreto 1066/2001, de 28 de septiembre, por el que se aprueba el reglamento que establece condiciones de protección del dominio público radioeléctrico, restricciones a las emisiones radioeléctricas y medidas de protección sanitaria frente a emisiones radioeléctricas. *Boletín Oficial del Estado*, Vol. 234, 36217–36227, September 2001.
6. Adane, Y., A. Gati, Man-Fa Wong, C. Dale, J. Wiart, and V. F. Hanna, "Optimal modeling of real radio base station antennas for human exposure assessment using spherical-mode decomposition," *IEEE Antennas Wireless Propag. Lett.*, Vol. 1, 215–218, 2002.

7. Alvarez, Y., C. Cappellin, F. Las-Heras, and O. Breinbjerg, "On the comparison of the spherical wave expansion-to-plane wave expansion and the sources reconstruction method for antenna diagnostics," *Progress In Electromagnetics Research*, PIER 87, 245–262, November 2008.
8. Alvarez, Y., F. Las-Heras, and M. R. Pino, "Reconstruction of equivalent currents distribution over arbitrary three-dimensional surfaces based on integral equation algorithms," *IEEE Trans. Antennas Propagat.*, Vol. 55, No. 12, 3460–3468, December 2007.
9. Alvarez, Y., F. Las-Heras, and M. R. Pino, "On the comparison between the spherical wave expansion and the sources reconstruction method," *IEEE Trans. Antennas Propagat.*, Vol. 56, No. 10, 3337–3341, October 2008.
10. Alvarez, Y., F. Las-Heras, M. R. Pino, and J. A. Lopez, "Acceleration of the sources reconstruction method via the fast multipole method," *IEEE Antennas and Propagation Society International Symposium 2008, AP-S 2008*, 1–4, July 2008.
11. Ziyat, A., D. Picard, L. Casavola, and J. C. Bolomey, "Prediction of BTS antennas safety perimeter from NF to NF transformation: An experimental validation," *Proc. Antenna Measurement Techniques Association Symposium (AMTA 2001)*, Denver, Colorado, USA, October 2001.
12. Balanis, C. A., *Advanced Engineering Electromagnetics*, John Wiley and Sons, New York, NY, 1989.
13. Bizzi, M. and P. Gianola, "Electromagnetic fields radiated by GSM antennas," *Electron. Lett.*, Vol. 35, No. 11, 855–857, May 1999.
14. Van Bladel, J., *Electromagnetic Fields*, John Wiley and Sons, New Jersey, NJ, 2007.
15. Blanch, S., J. Romeu, and A. Cardama, "Near field in the vicinity of wireless base-station antennas: An exposure compliance approach," *IEEE Trans. Antennas Propagat.*, Vol. 50, No. 5, 685–692, May 2002.
16. Cappellin, C., O. Breinbjerg, and A. Frandsen, "Properties of the transformation from the spherical wave expansion to the plane wave expansion," *Radio Sci.*, Vol. 43, 2008.
17. Cappellin, C., A. Frandsen, and O. Breinbjerg, "Application of the SWE-to-PWE antenna diagnostics technique to an offset reflector antenna," *IEEE Trans. Antennas Propagat.*, Vol. 50, No. 5, 204–213, October 2008.
18. Casavola, L., A. Ziyat, D. Picard, and J. C. Bolomey, "Rapid

- evaluation of electric and magnetic field radiated by base station antennas for cellular communication,” *Proc. XXVIIIth General Assembly of the International Union of Radio Science*, Maastricht, Netherlands, August 2002.
19. Casavola, L., A. Ziyyat, D. Picard, and J.-C. Bolomey, “Rapid determination of safety distances of a base station antenna for cellular communications,” *Proc. 5th International Congress of the European BioElectromagnetics Association, EBEA '2001*, 133–135, Helsinki, Finland, September 2001.
 20. Chao, H.-Y., C. Lin, K. Pirapaharan, and W. C. Chew, “Fast field calculation by a multilevel fast multipole algorithm for large complex radiators and scatterers,” *IEEE Antennas and Propagation Society International Symposium 2003*, Vol. 1, 35–38, Jun. 2003.
 21. Chew, W. C., *Waves and Fields in Inhomogeneous Media*, Van Nostrand Reinhold, John Wiley and Sons, New York, 1990.
 22. Cicchetti, R., A. Faraone, and Q. Balzano, “A uniform asymptotic evaluation of the field radiated from collinear array antennas,” *IEEE Trans. Antennas Propagat.*, Vol. 51, No. 1, 89–102, January 2003.
 23. Coifman, R., V. Rokhlin, and S. Wandzura, “The fast multipole method for the wave equation: A pedestrian prescription,” *IEEE Trans. Antennas Propagat.*, Vol. 53, No. 3, 7–12, June 1993.
 24. Cátedra, M. F., R. P. Torres, J. Basterrechea, and E. Gago, *The CG-FFT Method: Application of Signal Processing Techniques to Electromagnetics*, Artech House, Boston, 1995.
 25. Faraone, A., R. Y.-S. Tay, K. H. Joyner, and Q. Balzano, “Estimation of the average power density in the vicinity of cellular base-station collinear array antennas,” *IEEE Trans. Veh. Technol.*, Vol. 49, No. 3, 984–996, May 2000.
 26. Gatti, M. S. and Y. Rahmat-Samii, “FFT applications to planepolar near-field antenna measurements,” *IEEE Trans. Antennas Propagat.*, Vol. 36, No. 6, 781–791, June 1988.
 27. Las-Heras, F., M. R. Pino, S. Loredó, Y. Álvarez, and T. K. Sarkar, “Evaluating near-field radiation patterns of commercial antennas,” *IEEE Trans. Antennas Propagat.*, Vol. 54, No. 8, 2198–2207, August 2006.
 28. Lopez, Y. A., F. Las-Heras, and M. R. Pino, “Application of the adaptive cross approximation algorithm to the sources reconstruction method,” *3rd European Conference on Antennas and Propagation, EuCAP 2009*, 761–765, March 2009.

29. Lopéz, Y. A., F. L.-H. Andrés, M. R. Pino, and T. K. Sarkar, "An improved super-resolution source reconstruction method," *IEEE Trans. Instrumentation and Measurement*, Vol. 58, No. 11, 3855–3866, November 2009.
30. Persson, K. and M. Gustafson, "Reconstruction of equivalent currents using a near-field data transformation — With radome application," *Progress In Electromagnetics Research*, PIER 54, 179–198, November 2005.
31. Sarkar, T. K., E. Arms, and S. M. Rao, "Application of FFT and the conjugate gradient method for the solution of electromagnetic radiation from electrically large and small conducting bodies," *IEEE Trans. Antennas Propagat.*, Vol. 33, 635–640, May 1986.
32. Song, J. M., C. C. Lu, and W. C. Chew, "Multilevel fast multipole algorithm for electromagnetic scattering by large complex objects," *IEEE Trans. Antennas Propagat.*, Vol. 45, No. 10, 1488–1493, October 1997.
33. Taaghola, A. and T. K. Sarkar, "Near-field to near/far-field transformation for arbitrary near-field geometry, utilizing and equivalent magnetic current," *IEEE Trans. Electromagnetic Compatibility*, Vol. 38, 536–542, 1996.
34. Yaghjian, A., "An overview of near-field antenna measurements," *IEEE Trans. Antennas Propagat.*, Vol. 34, No. 1, 30–45, January 1986.